Journal of Renewable Materials

Tech Science Press

DOI: 10.32604/jrm.2024.045586

ARTICLE

Characterization and Selection of Microcrystalline Cellulose from Oil Palm Empty Fruit Bunches for Strengthening Hydrogel Films

Susi Susi[1,2,*], Makhmudun Ainuri[3,*], Wagiman Wagiman[3] and Mohammad Affan Fajar Falah[3]

[1]Department of Agroindustrial Technology, Faculty of Agriculture, Universitas Lambung Mangkurat, Jl A Yani Km 36, Banjarbaru, South Kalimantan, 70714, Indonesia

[2]Doctoral Programme of Agroindustrial Technology, Faculty of Agricultural Technology, Universitas Gadjah Mada, Jl Flora No. 1, Bulaksumur, Yogyakarta, 55281, Indonesia

[3]Department of Agroindustrial Technology, Faculty of Agricultural Technology, Universitas Gadjah Mada, Jl Flora No. 1, Bulaksumur, Yogyakarta, 55281, Indonesia

[*]Corresponding Authors: Susi Susi. Email: susi_tip@ulm.ac.id; Makhmudun Ainuri. Email: dun@ugm.ac.id

Received: 31 August 2023 Accepted: 29 December 2023 Published: 11 April 2024

ABSTRACT

Microcrystalline cellulose (MCC) is one of the cellulose derivatives produced as a result of the depolymerization of a part of cellulose to achieve high crystallinity. When implemented in other polymers, high crystallinity correlates with greater strength and stiffnes, but it can reduce the water-holding capacity. The acid concentration and hydrolysis time will affect the acquisition of crystallinity and water absorption capacity, both of which have significance as properties of hydrogel filler. The study aimed to evaluate the properties and select the MCC generated from varying the proportion of hydrochloric acid (HCl) and the appropriate hydrolysis time as a filler for film hydrogel. MCC was produced by hydrolyzing cellulose of oil palm empty fruit bunches (OPEFB) with the HCl solution at varied concentrations and periods. The results show that the longer hydrolysis times and higher HCl concentrations increase crystallinity and density while lowering yield and water absorption. The extensive acid hydrolysis reduces the amorphous area significantly, allowing the depolymerization to occur and extend the crystalline area. The morphological properties of the MCC, which are smaller but compact, indicate the presence of disintegrating and diminishing structures. A 2.5 N HCl concentration and a 45-min hydrolysis time succeed in sufficient crystallinity as well as maintaining good water absorption capacity. The treatment produced MCC with absorption capacity of 4.03 ± 0.26 g/g, swelling capacity of 5.03 ± 0.26 g/g, loss on drying of 1.44% ± 0.36, bulk and tapped density of 0.27 ± 0.031 g/cm^3 and 0.3 ± 0.006 g/cm^3, respectively, with a crystallinity index of 88.89% ± 4.76 and a crystallite size of 4.23 ± 0.70 nm. The MCC generated could potentially be utilized as a hydrogel film filler, since a given proportion will be able to maintain the strength of the hydrogel, not readily dissolve but absorb water significantly.

KEYWORDS

Acid hydrolysis; hydrogel; OPEFB; microcrystalline cellulose; water absorption

1 Introduction

Cellulose is one of the main components in lignocellulosic biomass, usually representing 40%–70% of the dry mass of the material. Oil palm empty fruit bunches (OPEFB) is a lignocellulosic material containing

32.97% cellulose, 31.51% hemicellulose, and 19.79% lignin [1]. In the lignocellulosic matrix, cellulose molecules as microfibrils are a series of linear β (1,4)-glucan chains and have a small size [2,3]. The hydroxyl group (OH) in cellulose causes the stability and crystallinity of cellulose. Cellulose fibrils will form intra and intermolecular hydrogen bonds with one another, which will strengthen the crystalline structure [4]. Nature cellulose that has been purified from impurities such as wax, hemicellulose and lignin through a hydrolytic reaction process is called α-cellulose. A certain amount of α-cellulose must be obtained so that microcrystalline cellulose (MCC) and nanocellulose can be produced from lignocellulosic residues [5].

MCC obtained from a variety of sources using various processes and conditions will have characteristic differences including surface area, crystallinity, water content, porous structure, molecular weight, and particle size. MCC extraction involves two main processes of cellulose purification followed by acid hydrolysis. Both treatments affect the morphology, crystallinity, and thermal stability of the resulting MCC, all these properties are interestingly studied to apply these materials in the polymer matrix. Extensive MCC production studies are necessary depending on the source of lignocellulosic materials used, as well as compliance with MCC specifications for applied products [4].

In the hydrolysis method, the naturally solid cellulose microcrystals will be fragmented because the attached amorphous cellulose is dissolved. Several approaches are applied to the production of MCC and lead to various types of micromaterials. This depends on the source of cellulose, the treatment condition, and the disintegration process. These factors will give differences in crystallinity, water content, external surface, porous structure, particle size, and molecular weight. Among all methods, the acid hydrolysis method is widely used in MCC production on an industrial scale.

MCC can be produced from any material that contains high cellulose. MCC has been synthesized from several cellulosic materials including agricultural waste [6], *Posidonia oceanica* brown algae [7], bagasse and rice straw [8], sawdust waste [9], cotton [10], soybean skin [11], manau rattan [12], palm fiber [13], rice husk [14], corncob [15,16], bamboo betung [17], banana fiber (*Musa balbisiana)* [18], red seaweed [19], coconut fiber [20], conocarpus fiber [21], OPEFB fiber [22–25].

The manufacture of MCC began with the hydrolysis process, but many modification processes such as reactive extrusion, radiation-enzymatic, acid hydrolyze, and so on have been studied in the literature. Several methods have been performed including acid hydrolysis [19,25], chemomechanical processes [26], simultaneous ultrasonic and alkaline treatment [23], steam-hydrolysis of acids [24], reactive extrusion [11,27], and hydrothermal [28].

Acid hydrolysis is considered to be the most effective for eliminating lignin. The type and concentration of acid, reaction time, and temperature are the most important parameters to be controlled during hydrolysis [29]. Acid hydrolysis is an easy process to reduce particle size, increase crystallinity, and improve the mechanical properties of a lignocellulosic material after bleaching [30]. This condition occurs because the acid attacks the amorphous areas of the fiber, and the mostly crystalline remains insoluble in the acid [31].

MCC offers nontoxicity, good mechanical strength, low density, a large surface area, biodegradability, and biocompatibility. MCC is widely utilized as a thickening, bonding, and adsorbent in the pharmaceutical and cosmetic fields, as well as gel-forming agents, stabilizers, and anticaking agents in the food and beverage industries [32]. MCC are often characterized by a high degree of crystallinity, with varied values ranging from 55%–80% as assessed by X-ray diffraction (XRD). Furthermore, due to its crystallinity, MCC is insoluble in organic solvents and water. MCC is used as a hydrogel filler to improve the mechanical robustness of the hydrogel film so that it does not disintegrate readily.

Several research used commercial MCC specifications to investigate the usage of MCC in hydrogels [33–37], filler of biocmposites film [30,38–41], and filler of membrane [42]. This research review offers an overview of the utilization of MCC generated from OPEFB waste as a raw material in the production

of hydrogel films. It should be mentioned that the properties of OPEFB fiber differ from those of other fibers, resulting in various crystallinity standards. Similarly, acid concentration and hydrolysis time will have an impact. As a result, particular information on the parameters of the acid hydrolysis process on cellulose from OPEFB is required, which can indicate the acceptability of the MCC product for use in hydrogel films.

MCC has been extensively used in medicinal industries, although research into MCC as a filler on hydrogel film is still limited. The research's distinctiveness verifies the necessity for OPEFB-based MCC with water absorption, swelling, and crystallinity features to make hydrogel films with strong water absorbent capacity and non-melting structure. As a result, the acidic concentration and extended hydrolysis will impact the crystallinity of the MCC, resulting in some modifications in the MCC's properties. Subsequently, the precise properties of the OPEFB base MCC are essential for the hydrogel film, which will definitely be affected by the acid concentrations and length of hydrolysis utilized. The right process parameters are selected to produce MCC with the high swelling and water absorption capacity that remains considered and high crystallinity to enable its usage as a filler in hydrogel films. A hydrogel film requires to have strong water absorption capabilities. MCC, the filler with a high degree of crystallinity, is required to sustain the hydrogel's mechanical strength and prevent it from dissolving or tearing readily.

Most commercial MCC is produced from cotton; therefore, the production of OPEFB waste-based MCC from the palm oil industry strongly supports the circular economy. The novelty of the research is to find the MCC characteristics of OPEFB at the appropriate HCl concentration and hydrolysis periods that are suitable for the requirements of hydrogel film use. Extensive research has been conducted on the properties of MCC, with a primary focus on its efficacy as a binder or filler in tablets. The tablets must be able to form compact shapes when compressed, which makes MCC an ideal choice due to its exceptional properties. When it comes to tablet production, MCC is a crucial binder due to its excellent characteristics in terms of porosity, crystallinity, and particle size [43]. In the use of MCC as a hydrogel filler, the determination of characteristics will be based on the balance of water absorption ability and swelling power to support the nature of the hydrogel film with a large water absorption ability. Hydrogel film with MCC filler also considers the crystallinity index of MCC itself so that the hydrogel is able to absorb large amounts of water while still maintaining its mechanical strength without tearing or dissolving easily.

This research aimed to find the best properties of MCC for use as a filler in a hydrogel film. The hydrogel film used as a biowrapping or an absorbent on fresh fruit and vegetables should be able to absorb the amount of water emitted by the respiration and transpiration processes. As a result, in setting the process parameters for the optimum MCC, the balance of the ability to absorb moisture and not readily dissolve on the hydrogel film becomes essential.

2 Materials and Methods

2.1 Materials

OPEFB were supplied from PT Batu Gunung Mulia Putra Agro (BGMPA) South Kalimantan, NaOH (Merck), $NaClO_2$ (Clover Chemicals Ltd., Bridge, England), glacial acetic acid (Merck), HCl (Merck), MCC commercial (Sigma Aldrich) and distilled water. The equipment includes a beaker glass, measuring cup, centrifuge, hotplate stirrer, spatula, filter paper, filter cloth, grinder (Getra IC-06B, China) oven (Memmert, Germany), and X-Ray Diffraction (Rigaku MiniFlex Hypix-400MF 2D HPAD detector, Japan), Attenuated Total Reflectance-Fourier Transform Infrared Spectroscopy (ATR-FTIR) (Bruker 200546 Model Alpha, Australia), Scanning Electron Microscopy (SEM) (Brand FEI Inspect-S50 type, Japan), and Simultaneous Thermogravimetry Differential Thermal Analyzer-Differential Scanning Calorimetry (TGA-DT-DSC) NEXTA STA (Hitachi STA200RV with Real View Sample Observation, UK), and Universal Testing Machne (Zwick type z0.5kN, Germany).

2.2 Experimental Design

The MCC produces OPEFB cellulose and utilizes a random set of two-factor experimental designs that comprise HCl solution factors with varying concentrations and extended hydrolysis times. The following are the detailed treatment factors:

1. HCl solution concentrations: 1.5, 2.5, 3.5 N.
2. Hydrolysis time: 15, 30, 45, and 60 min.

2.3 Preparation of OPEFB

OPEFB was washed with clean water, manually separated the fibers, and then rinsed for up to 4 cycles using clean water. The OPEFB was then immersed in hot water (±100°C) for 1 h to facilitate the release of fibrous oil residue. OPEFB fibers were soaked with a 2% soap solution with a ratio of fibers and soap solution 1:4 to remove residual oil and dust for 5 h, then rinsed with clean water. The clean OPEFB fibers were drained and dried in an oven at 60°C for 48 h. Dried OPEFB fibers, cut into 5 cm, then milled and sieved to 30 mesh.

2.4 Bleaching and Delignification Process

10 g of OPEFB fibers was bleached twice using 3.22% $NaClO_2$ with a 1:25 w/v temperature of 70°C–80°C for 1 h. The bleached fibers are dried and weighed. The bleached fibers were delignified using a 10% NaOH solution with a ratio of 1:20 (w/v) at room temperature (30°C). The delignified cellulose was washed with distilled water. The cellulose was refluxed for 30 min with distilled water for washing and then dried at 60°C for 24 h.

2.5 Production of MCC

OPEFB cellulose was hydrolyzed using 1.5N, 2.5N, and 3.5N HCl solutions at 100°C ± 2°C for 15, 30, 45, and 60 min with a ratio of cellulose: HCl solution 1:30. The obtained MCC was filtered and washed using distilled water until neutral. MCC was dried at 60°C for 24 h. The obtained MCC was grounded to make powder.

2.6 Production of Hydrogel

The hydrogel is produced by combining a 3% MCC solution and a 3% CMC solution with a citric acid crosslinker. MCC 3% is prepared by dissolving 3 grams of MCC in a 6/4/90 ionic solution of NaOH/urea/water, whereas CMC 3% is made by dissolving it in aquades. MCC 3% solution and CMC 3% solution are mixed in a 90:10 and 80:20 ratio, respectively, and 10% glycerol (v/v) is added from the MCC/CMC mixture. The solution is mixed at room temperature, and then monohydrate citric acid is added as a 5% (b/v) crosslinker of the mixture of MCC and CMC solutions. For two hours, the solution was mixed to room temperature. The hydrogel solution is frozen for 24 h (−2°C) and then thawed at room temperature until it melts. The casting technique involves pouring the solution into a glass cup and crosslinking it for 24 h at a temperature of 80°C to produce a hydrogel film.

2.7 Characterization of MCC and Hydrogel

MCC was tested, including yield, loss of drying, bulk and tapped density, water absorption capacity, and swelling capacity. The chemical structure of cellulose was analyzed by Attenuated Total Reflectance-Fourier Transform Infrared Spectroscopy (ATR-FTIR) (Bruker 200546 Model Alpha), crystallinity analysis was carried out by X-Ray Diffraction (XRD) (Rigaku MiniFlex Hypix-400MF 2D HPAD detector), while the morphology analysis of MCC using Scanning Electron Microscopy (SEM) Brand FEI Inspect-S50 type, thermal properties using Simultaneous Thermogravimetry Differential Thermal Analyzer-Differential

Scanning Calorimetry (TGA-DT-DSC). Tensile strength hydrogel measured based on ASTM D882 using Universal Testing Machne (Zwick type z0.5kN, Germany).

2.7.1 Loss on Drying

MCC initial (a) dried in an oven at 105 C for 24 h. MCC after drying weighed (b) and drying loss calculated by determining the amount of weight reduction after drying. Loss of drying was calculated using Eq. (1).

$$Loss\ on\ drying\ (\%) = \frac{a-b}{a} x\ 100\% \tag{1}$$

2.7.2 Bulk and Tapped Density

5 g of the MCC sample was weighed, put into a 50 mL measuring cup, leveled the surface, and read the volume. The bulk and tapped density were calculated as the ratio of the sample weight to the volume read on the measuring cup and volume after 500 tapps [44]. The tapped volume was determined by dropping/tapping the cylinder on a flat wooden platform from a height of about 2–3 cm at 2–3 s intervals until there was no further reduction in the volume of the material. Bulk density and tapped density were calculated by Eq. (2).

$$Density\ \left(g/cm^3\right) = sample\ weight\ (g)/volume\ \left(cm^3\right) \tag{2}$$

2.7.3 Water Absorption Capacity and Swelling Capacity

The centrifuge tube with known weight (c) was filled with 0.2 g of MCC (a), then 10 mL of distilled water was added and vortexed. Then it was left for 30 min, centrifuged at 3500 rpm for 10 min, and decanted and weighed (b) [44]. Water absorption capacity and swelling capacity were calculated by Eqs. (3) and (4).

$$Water\ absorption\ capacity\ (g/g) = \frac{b-a}{m} \tag{3}$$

$$Swelling\ capacity\ (g/g) = \frac{b-c}{m} \tag{4}$$

a = dry sample weight + centrifuge tube weight (g).

b = weight of sample that has been wetted + centrifuge tube weight (g).

c = centrifuge tube weight (g).

m = sample weight (g).

2.7.4 Swelling and Ensile Strength of Hydrogel

The weighted hydrogel mass is immersed in the swelling medium of aquades pH 7 ± 0.5, during 24 h, the swollen gel is wiped with filter paper, the hydrogel is removed and then immediately weighed. The swelling is calculated using the following Eq. (5). Tensile strength of hydrogel was determined using an ASTM D882 by universal tensile machine.

$$Swelling\ (\%) = \frac{Ws}{Wt}\ x\ 100\% \tag{5}$$

where Ws is the weight of the swelling hydrogel, and Wt is the dry weight of hydrogel.

2.7.5 Fourier Transform Infrared Spectroscopy

Fourier transforms infrared (FT-IR) spectra were acquired on an Attenuated Total Reflectance-Fourier Transform Infrared Spectroscopy (ATR-FTIR) (Bruker 200546 Model Alpha) using KBr discs. With a

resolution of 2 cm^{-1}, the scanned range was 4,000 to 400 cm^{-1}. The peak areas were integrated using the OriginPro program.

2.7.6 X-Ray Diffraction

X-ray diffraction (XRD) was carried out to study sample crystallinity. The sample patterns of all cellulose samples were pressed to form pellets and recorded on an X'Pert X-ray diffractometer using Ni-filtered Cu Kα radiation (30 kV and 30 mA). The diffraction intensity was measured between the Bragg angle (2θ) of 3°–90°. Scan speed of 10°/min, step width of 0.02°. The crystallinity index (CrI) was calculated by the Segal formula at Eq. (6) [45].

$$CrI\ (\%) = (I_{002} - I_{am})/I_{002}\ x\ 100 \tag{6}$$

where I_{002} indicates the maximum intensity of the 002 peaks around 2θ = 22.0°–23.0°, and I_{am} is the lowest intensity corresponding to the value of 2θ around 15.0°–17.0°.

The d-spacings were calculated using Bragg's equation (Eq. (7)) and the crystallite sizes were calculated from the Scherrer equation as follows:

$$L = \frac{K\lambda}{\beta} cos\theta \tag{7}$$

where L is the size of crystallite (nm), K is the Scherrer constant (0.94), λ is the X-ray wavelength (0.15418 nm), β is the FWHM (full-width half maximum) of the lattice plane reflection in radian, and θ is the corresponding Bragg angle (reflection angle).

2.7.7 Thermal Properties

The thermal properties of the MCC samples were examined using Thermogravimetry (TG), Differential Thermogravimetry (DTG), and Differential Scanning Calorimetry (DSC) on Simultaneous Thermogravimetry Differential Thermal Analyzer-Differential Scanning Calorimetry (TGA-DT-DSC) (NEXTA STA (Hitachi STA200RV with Real View Sample Observation). Samples weighing between 3 and 10 mg were utilized. Each sample was heated from ambient temperature (30°C) to 550°C at a rate of 5°C/min under nitrogen 100 mL/min.

2.8 Data Analysis

The quantitative data was evaluated using variance analysis (ANOVA) at a 5% error rate (α = 0.05), and if the treatment factor had significant effects, the Duncan Multiple Range Test (DMRT) was used to determine the distinction in treatment. The data was analyzed using IBM SPSS Statistics version 24. Data of FTIR, XRD, TG, DTG and DSC were analyzed by OriginPro program. Qualitative data were presented descriptively.

3 Results and Discussion

MCC is derived from the α-cellulose structure, which is insoluble in NaOH 17.5% solution. It is known that OPEFB fibers used as raw materials for MCC contain hemicellulose of 31.51%, cellulose of 32.97%, and lignin of 19.79%. Following the acid bleaching process in two phases and base delignification can greatly reduce impurities of hemicellulose and lignin. OPEFB-derived cellulose includes 83.0% cellulose, 9.30% hemicellulose, and 1.70% lignin. MCC is a cellulose derivative material that has the potential to evolve into a polymer composite. α-cellulose OPEFB extraction results vary from 83% to 94% [1] indicating that it has the potential to be developed into MCC. MCC is a partially hydrolyzed and depolymerized cellulase product with irregular amorphous areas [46]. The acid hydrolysis technique is used to process the OPEFB cellulose with concentration variations of 1.5, 2.5, and 3.5 N and extended hydrolyzing

periods ranging from 15, 30, 45, and 60 min. The conversion of OPEFB cellulose into MCC is illustrated in Fig. 1.

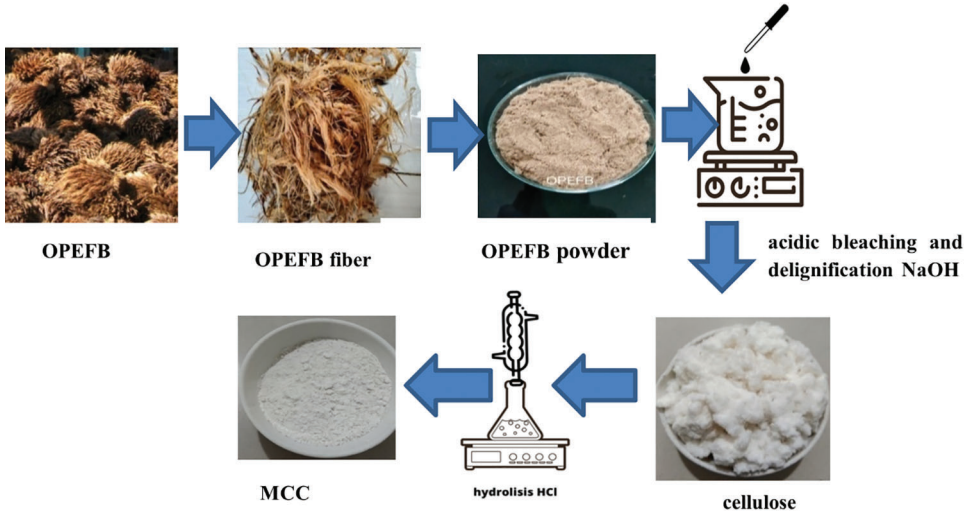

Figure 1: Process step of MCC from OPEFB

The acid hydrolysis process that converts OPEFB-based cellulose to MCC causes a variety of changes in the cellulose. The most noticeable change is that the cellulose structure will be shorter, which will correlate with the increased density as well as the shape on the rougher cellulosa surface. SEM is capable of illustrating the size of minute crushed cellulose particles. Acid hydrolysis will also eliminate the amorphous structure of hemicellulose as well as lignin. This relates to MCC having a higher crystallinity index than cellulose. Similarly, MCC crystals are greater in size than cellulose.

The structure and properties of MCC vary depending on the origin of the cellulose and the hydrolysis parameters used, such as temperature, hydrolyze time and acid concentration. MCC was chosen as a filler for film hydrogel products in this investigation. It should be emphasized that the MCC employed should sustain the hydrogel's stiffness while also having a high moisture absorption capacity. To acquire such features, the acid concentration and hydrolysis time must be known.

Cellulose microfibrils lack a regular surface because they are composed of crystalline and amorphous areas. The cellulose chains in amorphous regions are randomly aligned in a long straight pattern, resulting in a reduced density in these noncrystalline regions. As a result, acid attack is possible in the amorphous area. Hydronium ions can penetrate the cellulose chains of these amorphous domains, causing hydrolytic fragmenting of glycoside bonds and, finally, the disintegration of individual crystals. Due to free movement following hydrolytic splitting, these crystals can grow in size. This implies that MCC crystallites were larger in dimension than the original microfibrils [47].

3.1 Yield and Loss on Drying

The acid hydrolysis method used in the MCC process will diminish the cellulose mass. The acid will degrade part of the cellulose structure, the amorphous part, leaving the crystalline part. The intensity of depolymerization depends heavily on the acid concentration and the hydrolysis length. Table 1 shows that the higher the concentration of HCl and the longer the hydrolysis will further reduce the yield of MCC. Cellulose hydrolysis with 1.5 N HCl provides MCC in the 80–90% range, although yield decreases at

higher HCl concentrations. MCC yields range from 70% to 80% when using a concentration of HCl 3.5 N. The yield of MCC decreases with rising HCl concentrations and extended hydrolysis, as shown in Figs. 2a and 2b. The acid hydrolysis process will degrade some cellulose components, particularly the amorphous fragments of hemicellulose and lignin. The more intensive the hydrolysis, the greater the cellulose mass decrease and the increased cellulose crystalline component of the cellulose.

Table 1: Data of yields and loss of drying MCC

Hydrolysis time (min)	MCC yields (%)			Loss on drying (%)		
	HCl 1.5 N	HCl 1.5 N	HCl 1.5 N	HCl 1.5 N	HCl 1.5 N	HCl 1.5 N
15	$92.95^{a} \pm 0.34$	$87.77^{a} \pm 0.22$	$83.40^{a} \pm 0.72$	1.21 ± 0.31	1.96 ± 0.05	2.92 ± 0.41
30	$89.37^{b} \pm 1.60$	$85.26^{b} \pm 0.84$	$79.59^{b} \pm 1.06$	0.73 ± 0.02	0.96 ± 0.00	2.18 ± 0.72
45	$86.06^{c} \pm 1.11$	$81.30^{c} \pm 0.36$	$77.44^{c} \pm 0.30$	1.45 ± 0.02	1.44 ± 0.36	3.37 ± 0.68
60	$85.89^{d} \pm 0.67$	$79.82^{d} \pm 0.19$	$74.74^{d} \pm 0.22$	2.44 ± 0.40	0.98 ± 0.03	2.17 ± 0.34

Note: Different letters in the same column indicate significantly different treatments ($p \leq 0.05$).

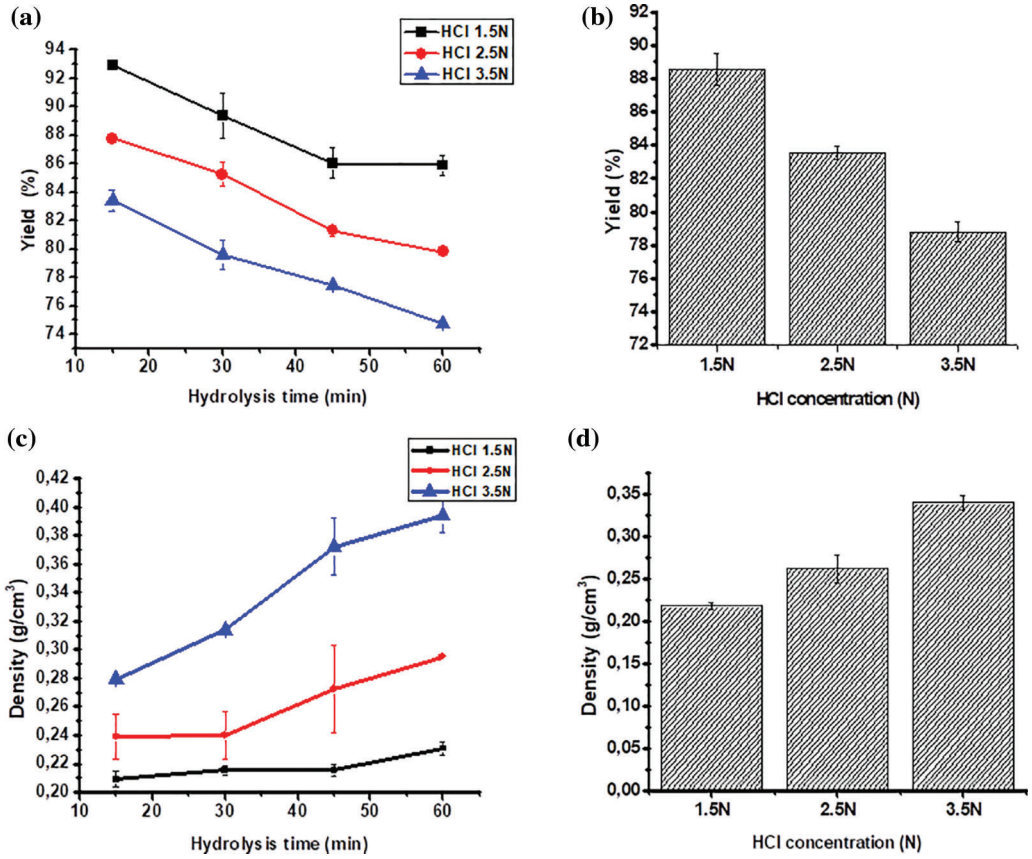

Figure 2: The effect of hydrolysis time anc HCl concentration on yield (a, b); and density (c, d)

MCC suffers from drying loss due to moisture loss, with MCC hydrolysis results of HCl 3.5 N showing more significant drying losses than concentrations of 1.5 and 2.5 N. Drying loss rates vary but tend to be above 2% at HCl 3.5 N concentrations, while 1%–2% at HCl 1.5 and 2.5 N concentrations. MCC

commercial has a loss on drying specifications of less than 7%, and the resulting OPEFB-based MCC passes the specifications.

When MCC is used as a binder or filler in granulation, its moisture content impacts cohesiveness. The compaction properties of MCC are insensitive to humidity fluctuations below 3% moisture content. Increasing the water content to a suitable level will usually boost the material's binding strength. Moisture can boost the strength of a material's van der Waals bond, but with over 3% water content, the bond strength decreases because the hydrogen bonds linking the hydroxyl groups in the cellulose chain are disrupted. Increasing the free water content reduces the intermolecular forces of attraction, allowing particle dispersion [48]. The mechanical properties of MCC change considerably when the moisture content surpasses 5%–6%; at greater moisture content, bond strength, and compaction decline.

3.2 Bulk and Tapped Density

MCC, a result of acid hydrolysis, has partially depolymerized, indicating a high crystalline structure. The crystalline structure will support the mass density of the MCC. The higher the HCl concentration the longer the hydrolysis time, resulting in higher bulk density ($p \leq 0.05$) and tapped density (Table 2).

Table 2: Data of bulk and tapped density of MCC

Hydrolysis time (min)	Bulk density (g/cm^3)			Tapp density (g/cm^3)		
	HCl 1.5 N	HCl 1.5 N	HCl 1.5 N	HCl 1.5 N	HCl 1.5 N	HCl 1.5 N
15	$0.21^{a} \pm 0.005$	$0.24^{a} \pm 0.016$	$0.28^{b} \pm 0.001$	$0.24^{a} \pm 0.017$	$0.26^{a} \pm 0.000$	$0.32^{bcd} \pm 0.006$
30	$0.22^{a} \pm 0.003$	$0.24^{a} \pm 0.016$	$0.31^{c} \pm 0.001$	$0.25^{a} \pm 0.022$	$0.28^{ab} \pm 0.022$	$0.35^{c} \pm 0.016$
45	$0,22^{a} \pm 0.003$	$0.27^{b} \pm 0.031$	$0.37^{d} \pm 0.020$	$0.24^{a} \pm 0.022$	$0.31^{bc} \pm 0.006$	$0.40^{d} \pm 0.023$
60	$0.23^{a} \pm 0.005$	$0.30^{bc} \pm 0.001$	$0.39^{d} \pm 0.012$	$0.25^{a} \pm 0.016$	$0.33^{cd} \pm 0.001$	$0.43^{d} \pm 0.012$

Note: Different letters in the same column indicate significantly different treatments ($p \leq 0.05$).

A higher density signifies a lower volume level within the same unit mass. This implies that MCC hydrolyzed at HCl 3.5 N has a higher density. MCC hydrolyzed at HCl 2.5 N with hydrolysis times of 45 and 60 min exhibited bulk density and tap density similar to hydrolyzed MCC at HCl 3.5 N with hydrolysis times of 15 and 30 min.

The MCC density rises as the acid hydrolysis length increases, this phenomenon can be seen in Figs. 2c and 2d. The density characteristics are utilized to provide an overview of MCC's compression and density, mainly if MCC is employed as a solid product filler. Adding MCC with high-density characteristics leads to a lower volume since it is more compact, as shown by the tap density.

MCC has a relatively low density, and MCC based on OPEFB is similar to MCC based on other material sources. The bulk density of *Gossipium herbaceum*-based MCC is 0.37–0.53 g/cm^3, and the tapped density is 0.47–0.60 g/cm^3, whereas MCC of Avicel PH 102 has a bulk density of 0.31 g/cm^3 and a tapped density of 0.38 g/cm^3 [49].

3.3 Water Absorption Capacity and Swelling Capacity

MCC is commonly used as a filler in various products to improve density and sturdiness. MCC is added to tablets to boost their binding capacity and reduce disintegration. MCC is used as a filler in the use of hydrogels to maintain the strength of the hydrogel, which is naturally easy to absorb water.

Water absorption in the hydrogel above its capacity causes the hydrogel to soften. MCC as a hydrogel filler necessitates a balance of properties as an absorbent and a hydrogel structural stabilizer. Tables 3 and 4

illustrate how each HCl concentration and hydrolysis time affected water absorption and swelling capacity. Increasing the HCl concentration to 3.5 N reduced water absorption and swelling capacity. Fig. 3 illustrates these phenomena. The same result is obtained by increasing the hydrolysis duration to 60 min. The hydrolysis of *Gossipium herbaceaum* cellulose in 2.5 N HCl for 15 min produced an MCC with a hydration capacity of 2.55–2.86 [49], and the MCC of OPEFB had a slightly higher water absorption capacity (Table 3) than Avicel PH 102, which was 3.55. Reduced hydroxyl in the acid hydrolysis process and higher structural crystallinity in MCC can both induce a decrease in water absorption capacity.

Table 3: Data of water absorption capacity of MCC

Hydrolysis time (min)	Water absorption capacity (g/g)			Mean
	HCl 1.5 N	HCl 2.5 N	HCl 3.5 N	
15	5.40 ± 0.14	4.49 ± 0.16	4.49 ± 0.16	4.57^{c} ± 0.74
30	4.86 ± 0.53	4.32 ± 0.84	4.32 ± 0.84	4.22^{b} ± 0.67
45	4.36 ± 0.11	4.03 ± 0.26	4.03 ± 0.26	3.85^{a} ± 0.58
60	4.14 ± 0.22	3.89 ± 0.09	3.89 ± 0.09	3.65^{a} ± 0.58
Mean	4.69^{c} ± 0.56	4.18^{b} ± 0.29	3.34^{a} ± 0.37	

Note: Different letters in the same column indicate significantly different treatments ($p \leq 0.05$).

Table 4: Data of swelling capacity of MCC

Hydrolysis time (min)	Swelling capacity (g/g)			Mean
	HCl 1.5 N	HCl 2.5 N	HCl 3.5 N	
15	6.30 ± 0.28	5.49 ± 0.16	4.79 ± 0.28	5.53^{c} ±0.70
30	5.86 ± 0.53	5.32 ± 0.13	4.47 ± 0.07	5.22^{b} ±0.67
45	5.36 ± 0.11	5.03 ± 0.26	4.15 ± 0.15	4.85^{a} ±0.57
60	5.14 ± 0.22	4.88 ± 0.93	3.94 ± 0.15	4.65^{a} ±0.58
Mean	5.67^{c} ± 0.54	5.18^{b} ± 0.29	4.34^{a} ± 0.37	

Note: Different letters in the same column indicate significantly different treatments ($p \leq 0.05$).

The changes in hydrogen bonding, the crystallinity of MCC, and the reduction of its amorphous part are significant factors in water absorption. As the crystallinity of MCC increases, its hydroxyl bonds and amorphous portion decrease, resulting in reduced water binding. Fick's law explains how a particle can move from one component to another due to differences in concentration or available space. Water is absorbed into MCC through a phenomenon similar to water diffusion since it occupies the available space. However, if MCC is more crystalline, the strong bonds make it difficult for water to diffuse into it.

The acid hydrolysis process will diminish the amorphous structure in cellulose, allowing for easier water binding. Cellulose's amorphous portions contribute significantly to water interactions. The hydration properties of cellulose are also strongly affected by the polymer's supramolecular structural features, which are very heterogeneous and include multiple regions with intermediate qualities (paracrystalline) in addition to crystalline and amorphous regions [50]. The paracrystalline area is a charged area created during drying by internal tension contraction and thermal characteristics [51]. When cellulose is exposed to water, the water is first dispersed in the cellulose microfibril matrix, causing significant swelling. This swelling will drastically alter the form and size of the absorbent pore structure. The presence of a

crystalline cellulose structure causes a minor absorption of water. The water absorption value can predict amorphocrystalline polymer crystallinity, which helps estimate their physicochemical properties and applications.

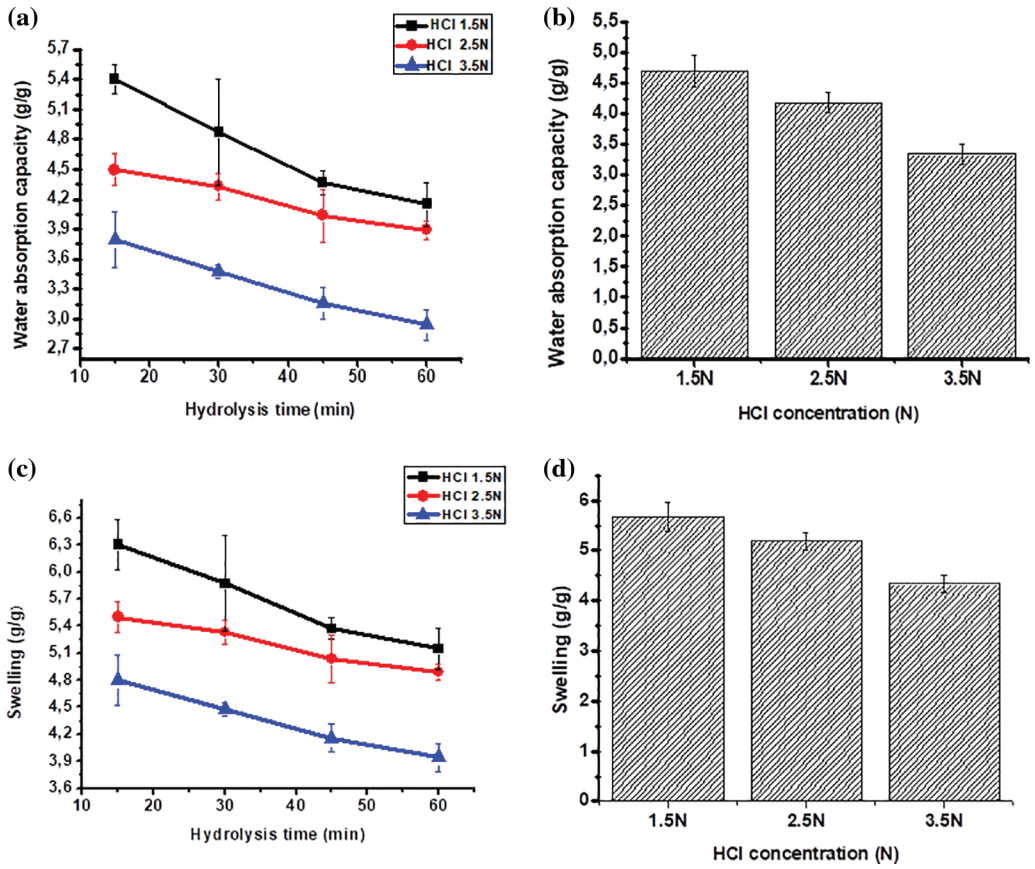

Figure 3: The effect of hydrolysis time and HCl concentration on water absorption capacity (a, b); and swelling (c, d)

Table 4 presents the swelling ability of the MCC derived from OPEFB, and it was observed that the more intense hydrolysis resulted in lower swelling capacity, which was in line with the decreased water absorption capacity. MCC volume increases due to particle swelling. The swelling time and water retention rate are primarily determined by the structural characteristics of MCC, such as density, porosity, and crystallinity [43]. MCC, although naturally hygroscopic and insoluble in water, exhibits expansion when it comes into contact with water. These characteristics are crucial if MCC is utilized as a filler for granulated products.

MCC is a type of water-insoluble filler known for its ability to swell and retain water well, which is also shared by calcium pectinate and sodium alginate fillers. When MCC is used as a filler in the wet granulation method, it absorbs water and becomes moist quickly. MCC also has the ability to retain moisture, which makes the wet mass less prone to overwetting caused by excess liquid during granulation [52]. The swelling ability of MCC is the key to enhancing the mechanical strength of the hydrogel, enabling it to retain water in the matrix without dissolving.

In using MCC in hydrogel films, the ability to absorb water is essential because MCC provides support for mechanical strength and maintains water absorption binding capacity. The mechanical strength of a

hydrogel will later be affected by the presence of a crystalline structure in the MCC. The larger the crystalline structure will affect the hydrogen bonding capacity of the hydroxyl structure in it so that the ability to absorb water decreases and the texture is not sturdy. As a result, the effectiveness of crosslinkers used in hydrogels to strengthen their bonds will also be reduced.

3.4 Fourier Transmittance Infrared Spectroscopy

The spectrum of various major functional groups in MCC is shown by FTIR analysis (Fig. 4). MCC's essential wavenumbers are 1035, 1313, 2897, and 3313 cm^{-1}. At a wavenumber of 1035 cm^{-1}, the OPEFB MCC is higher and sharper than the commercial MCC, and it is broader with a wavenumber of 3309 cm^{-1}. Meanwhile, OPEFB, cellulose, and MCC wavenumbers are underway to slope at 1252 cm^{-1}, 1629 cm^{-1}, and 2915 cm^{-1}, respectively. The decline in absorption from 1629 to 1252 cm^{-1} suggests that converting OPEFB fibers into cellulose and MCC removes a large percentage of lignin and hemicellulose [53], and intermolecular hydrogen bonding decreases at that wavenumber [54].

The FTIR spectrum demonstrates a shift in the crystal structure of cellulose to MCC by an increase in the crystalline band. Fig. 4 depicts the intensity intensification of 3309 cm^{-1} caused by OH stretching vibrations in hydrogen bonds. The properties of the MCC spectrum's hydrogen bond peaks are sharper than those of cellulose, which might be associated with the simplicity of intra and intermolecular hydrogen bonds. Similarly, the crystallinity band sharpens around 1312 cm^{-1} as a CH_2 bending vibration. Likewise, the peak at 1035 cm^{-1} has a higher intensity than cellulose due to ring vibrations and C-O-C bonds. The wavenumber area of 2897 cm^{-1} indicates the presence of an amorphous area, characterized by C-H stretching vibrations to a higher wavelength than the cellulose and declines in intensity in the spectrum band.

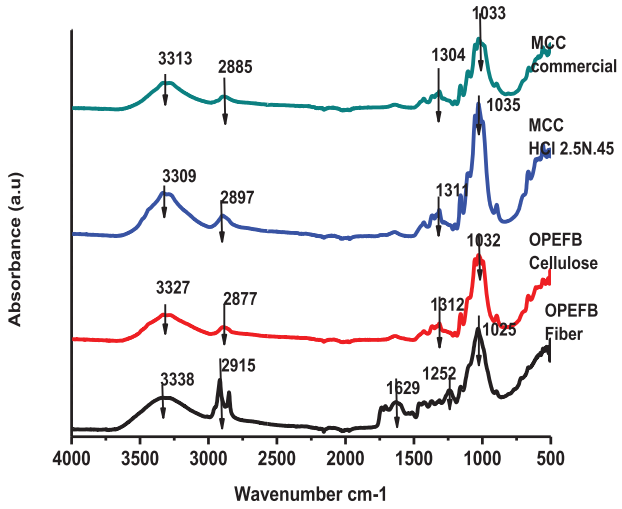

Figure 4: FTIR analysis of OPEFB fibers, cellulose, and MCC

3.5 X-Ray Diffraction

The hydrolysis of amorphous cellulose results in the formation of MCC, which increases the number of crystalline structures in cellulose. Acid hydrolysis with HCl causes partial destruction of disordered cellulose areas and breaks 1,4-glucan bonds to a certain degree of polymerization, resulting in a high degree of crystallinity [55]. In terms of yield, MCC yield loses linearly with acid concentration and hydrolysis time. This implies the presence of amorphous decay of the structure.

A crystalline structure in MCC correlates with a lower amorphous structural composition in cellulose. The amorphous structure enhances the ability to absorb water. The amorphous area of MCC is more hydrophilic than the crystalline component; hence, the absorbed water content is proportional to the amorphous fraction. MCC powder with a lower crystallinity level may contain more water than MCC powder with more crystals. MCC with a low degree of crystallinity will absorb water more easily because water absorption occurs in amorphous rather than crystalline areas.

Table 5 illustrates the way increasing the HCl concentration to 3.5 N and prolonging the hydrolysis time to 60 min impacts the crystallinity index of MCC. When cellulose is hydrolyzed with 2.5 N HCl, its crystallinity index rises, even though the acid hydrolysis periods of 45 and 60 min differ not appreciably (Figs. 5a and 5b). The higher the HCl content and the longer the hydrolysis period, the further the white cellulose turns cream, changing the hue of the final hydrogel.

Table 5: Data of crystallinity index of MCC

Hydrolysis time (min)	Crystallinity index (%)			Mean
	HCl 1.5 N	HCl 2.5 N	HCl 3.5 N	
15	71.25 ± 3.47	79.27 ± 8.79	79.37 ± 2.69	$76.63^{a\ b}$ ±6.05
30	70.60 ± 3.12	77.41 ± 0.53	75.87 ± 14.42	74.62^{a} ±7.33
45	82.00 ± 6.10	88.89 ± 4.76	83.48 ± 6.92	$84.79^{b\ c}$ ±5.66
60	83.60 ± 14.00	89.22 ± 6.43	88.51 ± 11.83	87.11^{c} ±9.11
Mean	76.86^{a} ±8.78	83.70^{a} ±7.31	81.81^{a} ±9.11	

Note: Different letters in the same column indicate significantly different treatments ($p \leq 0.05$).

The XRD analysis revealed the size of the crystallites in the resulting MCC. The size of the crystallites in MCC grows with increasing HCl concentration and hydrolysis length time (Figs. 5c and 5d). In line with the crystallinity index, the crystallite size of MCC produced by 2.5 N HCl hydrolysis tended to be more significant, and the hydrolysis times of 45 and 60 min produced crystallite sizes that were not significantly different (Table 6). Acid hydrolysis causes cellulose fragmentation and the breakdown of individual crystals. Free movement occurs after hydrolytic splitting, and these crystals can increase, leading to larger MCC crystals [47]. When compared to commercial MCC, OPEFB MCC has a similar crystallinity index. The analysis results show that MCC commercial has a crystallinity index of 89.52% and a crystallite size of 3.94 nm. Several lignocellulosic materials have been investigated for MCC conversion, with varying MCC crystallinity results. MCC based on rice husk has a CrI of 52.2% [14], MCC from *Saccharum spontaneum* has a CrI of 74.06% [56], MCC from oil palm frond has an index of 87% [13], MCC from OPEFB has CrI of 87% [22] and MCC from jute with CrI of 74.09% [57].

During hydrolysis, the acid will penetrate the amorphous region, causing the breakage of glycosidic linkages and the release of individual crystallites [47], which will grow and be ordered in parallel, increasing cellulose crystallinity [58]. The larger the crystallite size, the more extensive the hydrolysis. High crystallinity is influenced by the ability of the hydroxyl groups to form intramolecular and intermolecular hydrogen bonds in the cellulose chain to achieve a compact structure [59]. MCC with high crystallinity provides stiffness and strength when used as a filler in other polymers.

Cellulose has an amorphous phase with crystallographic planes centered at $2\theta = 18°$ and a crystalline phase with peaks located at 16°, 22°, and 34°. Fig. 6 shows MCC crystallinity with an average peak 2θ of 22.54° and a range of 2θ from 22.24° to 22.82°. MCC is sharper and greater in intensity than cellulose

or OPEFB fiber. Crystallinity is enhanced as intramolecular and intermolecular hydrogen bonding increases during the cellulose-to-MCC transformation [60]. The elimination of hemicellulose and lignin and an enhancement in tensile strength contribute to MCC's increased crystallinity [55]. High crystallinity MCC can be used as a preferred reinforcement material in preparing composite products [4] focused on hydrogel films in particular.

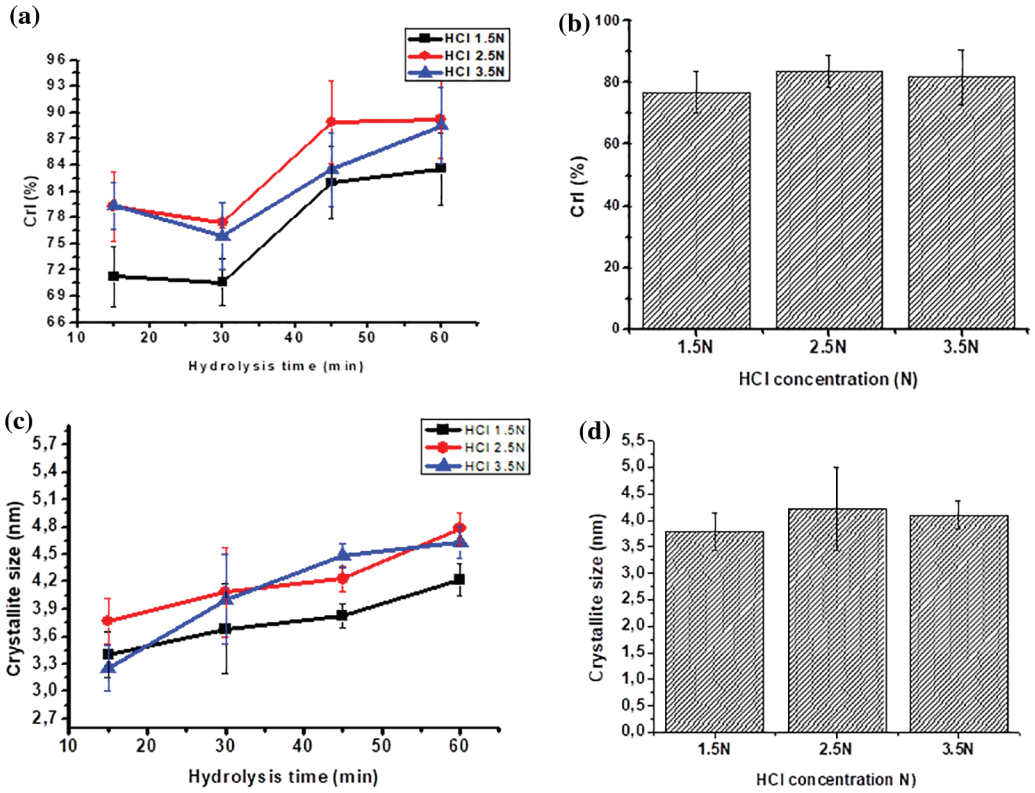

Figure 5: Effect hydrolysis time and HCl concentration on CrI (a, b), and crystallite size (c, d)

Table 6: Data of crystallite size of MCC

Hydrolysis time (min)	The crystallite size (nm)			Mean
	HCl 1.5 N	HCl 2.5 N	HCl 3.5 N	
15	3.40 ± 0.12	3.77 ± 0.93	3.25 ± 0.25	3.62^{a} ±0.44
30	3.68 ± 0.36	4.09 ± 0.80	4.00 ± 0.49	3.96^{ab}±0.42
45	3.83 ± 0.45	4.23 ± 0.70	4.49 ± 0.14	4.28^{bc}±0.44
60	4.22 ± 0.48	4.78 ± 0.71	4.63 ± 0.17	4.33^{c}±0.44
Mean	3.70^{a} ±0.35	4.37^{b}±0.35	4.06^{b}±0.56	

Note: Different letters in the same column indicate significantly different treatments ($p \leq 0.05$).

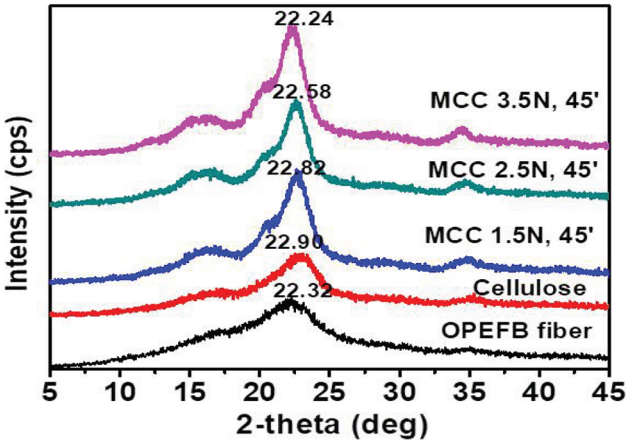

Figure 6: XRD analysis of OPEFB fibers, cellulose, and MCC

3.6 Scanning Electron Microscopy

Fig. 7 illustrates MCC's structural and morphological changes after 45 min of hydrolysis with HCl concentrations of 1.5, 2.5, and 3.5 N. Increasing the HCl concentration disintegrates the cellulose structure, which is crumbly and smaller when investigated at the same magnification as the structure at 3.5 N HCl concentration. The degradation of the cellulose structure expands more intensely as the concentration rises, as seen in the image with a magnification of 1000x. The diminishing yield and growing crystallinity index will demonstrate it. Because hemicellulose is less rigid than cellulose, deterioration and abrasion will occur first in the amorphous cellulose structure, particularly in the hemicellulose component, during hydrolysis. With increasing concentration and length of time, the breakdown will lead to the cellulose component and give rise to a greater crystalline structure.

The acid hydrolysis process breaks cellulose into tiny fragments, as shown in Fig. 7, where it is broken down into smaller pieces at a concentration of 3.5 N HCl. The acid treatment reduces the fibril structure's regularity and increases surface area with a significant degree of degradation. As a result of the hydrolysis of 3.5 N HCl concentrations, it seems that a more substantial number of fractures and fissures emerge on the MCC surface. The cracks form due to the rapid diffusion of acids into the cellulose structure, which decomposes the amorphous hemicellulose matrix and produces a dense structure containing patches of crystalline cellulose [15].

3.7 Thermal Properties

The thermograms of commercial MCC and OPEFB MCC hydrolyzed in 2.5 N HCl for 45 min, including TG and DTG, are shown in Fig. 8. The commercial MCC, a 5% mass reduction (onset temperature) decomposition process was obtained at a temperature of 298.14°C, while a 50% mass decomposition process was obtained at a temperature of 332.66°C. Compared to the OPEFB MCC, a 5% mass decomposition was obtained at 248.64°C, whereas 50% decomposition occurred at 336.19°C. The MCC OPEFB appears to have a higher amorphous structure. MCC loses mass at temperatures of 250°–375°C, with the maximum degradation occurring at 325°C [61]. The higher onset temperature suggests more thermal stability, which coincides with a high degree of crystallinity in MCC [62].

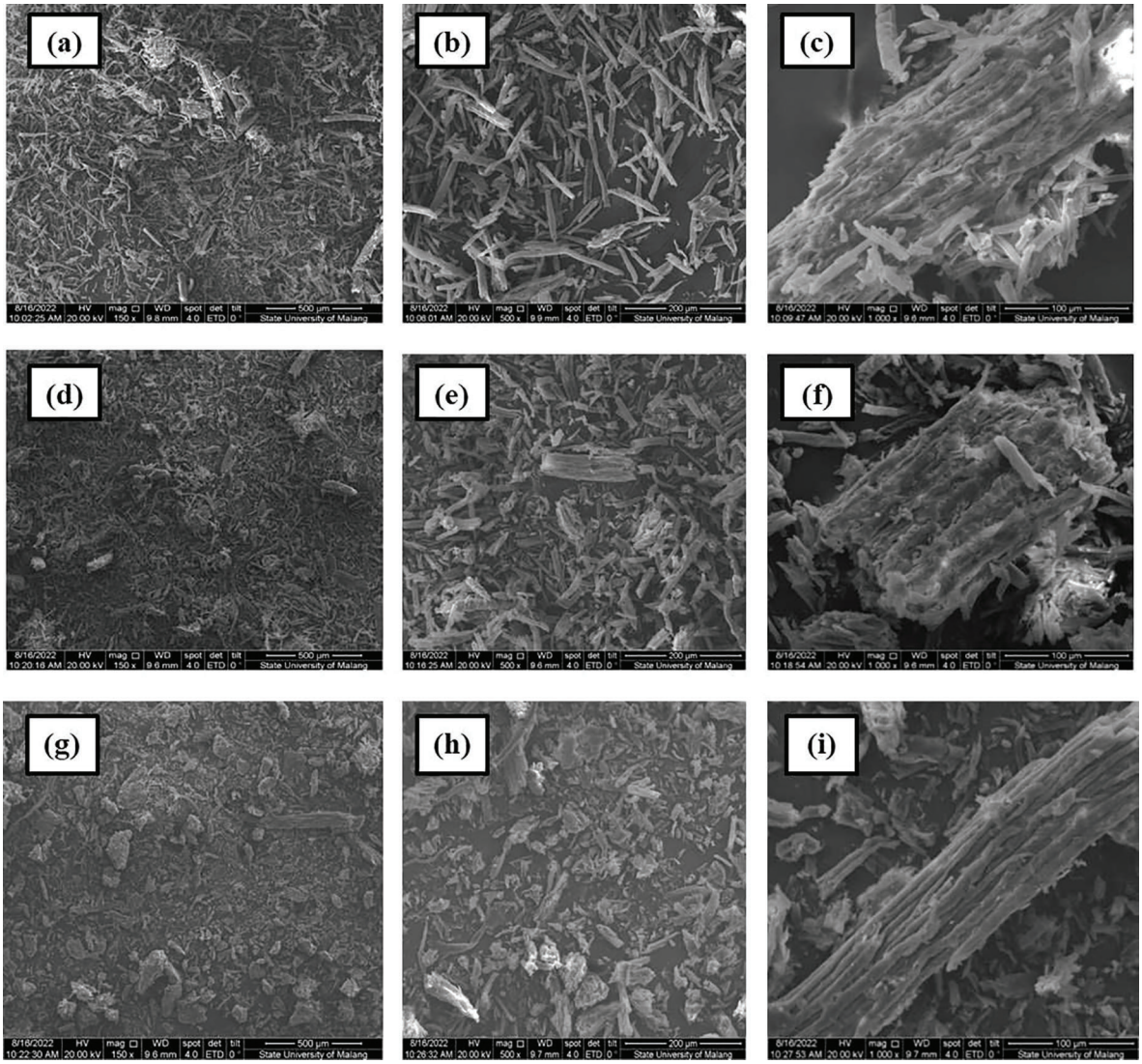

Figure 7: SEM analysis of MCC in magnification 150x, 500x and 1000x on N1.5T45 (a, b, c); N2.5T45 (d, e, f) and N3.5T45 (g, h, i)

The evolution of non-combustible gases such as CO_2, CO, formic acid, and acetic acid causes the first breakdown of cellulose. The fraction is thought to be lower in OPEFB MCC than in commercial MCC, resulting in a lower percentage of mass loss at the onset of degradation. Pyrolysis and the evolution of flammable gases occur in the second degradation stage at temperatures greater than 350°C. According to Fig. 8c, the DTG profile reveals that the MCC OPEFB structure's breakdown rate is higher at 350°C than commercial MCC. MCC OPEFB retains 3.65% of its residual at 550°C, while commercial MCC has 3.88%. This indicates that the commercial MCC and OPEFB MCC contain non-volatile carbon compounds robust to a wide range of pyrolysis temperatures. A detailed analysis of MCC's TG is presented in Table 7.

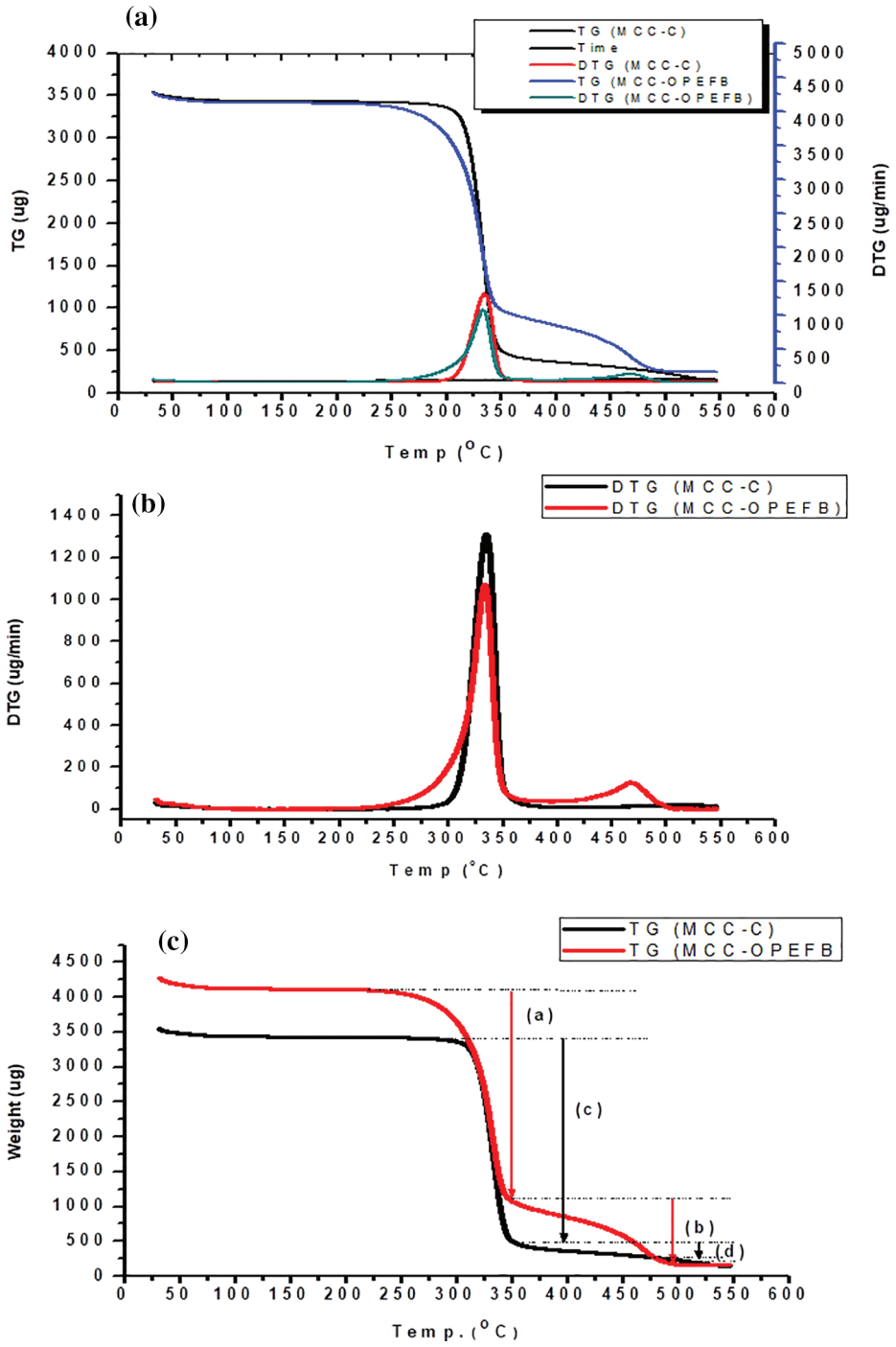

Figure 8: Analysis of TG and DTG of MCC of OPEFB and commercial MCC (MCC-C); (a) correlation TG and DTG; (b) DTG curve; (c) TG analysis curve

At temperatures above 350°C, OPEFB MCC has a sharper slope curve than commercial MCC, indicating that it decomposes more quickly. At this temperature, the mass reduction in commercial MCC was only 42.75%, reaching 85.19% in OPEFB MCC. The inclusion of anhydroglucose polymer chains will improve the intermolecular and intermolecular bonds, making the material stronger [63].

Table 7: Analysis TG of MCC

MCC of OPEFB				Commercial MCC			
Temp (°C)		Weight (μg)		Temp (°C)		Weight (μg)	
T1	233.00	W1	4123.00	T1	290.29	W1	3413.77
T2	350.00	W2	1128.00	T2	350.00	W2	487.35
T3	496.55	W3	167.00	T3	495.27	W3	279.14
ΔT_{1-2}	117.00	ΔW_{1-2} (a)	72.64%	ΔT_{1-2}	59.70	ΔW_{1-2} (c)	85.72%
ΔT_{2-3}	146.55	ΔW_{2-3} (b)	85.19%	ΔT_{2-3}	145.27	ΔW_{2-3} (c)	42.75%

The heat required to raise the sample and reference temperatures as a function of temperature is measured using Differential Scanning Calorimetry (DSC). The DSC test assesses the structural composition of glass and its glass transition properties, melting, and degradation temperatures. The OPEFB MCC contains two exothermic peaks at 350.07°C and 476.7°C, whereas the commercial MCC peak pattern begins with an endothermic peak. Fig. 9 illustrates the DSC analysis of OPEFB MCC and commercial MCC.

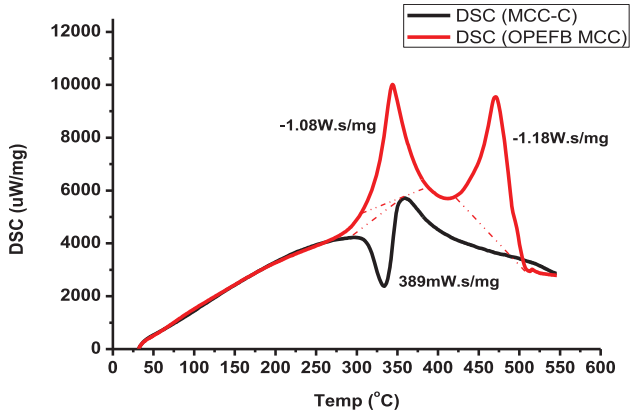

Figure 9: Analysis DSC of MCC of OPEFB and commercial MCC (MCC-C)

The negative peak on the commercial MCC indicates an uneven transition at 333.89°C, where melting occurs due to amorphous polymer breakdown. In OPEFB MCC, a positive and sharp crystallization peak forms, transitioning from cluttered to ordered, and a crystal is forming. Impurities are assumed to be responsible for the creation of two peaks.

Under certain conditions, continued acid hydrolysis can lead to the formation of unwanted reactive degradation products such as organic acids (such as formic acid, acetic acid, and butyric acid) and furans (such as hydroxy methyl furfural and furfural). These furans, along with oxycellulose, cellulose-reducing end groups, and linear monosaccharides, can react and create new products through Maillard reactions. Commercial MCC PH 102 may contain impurities, such as glucose, HCHO, and small amounts of hydrogen peroxide, which may affect the reactivity of microcrystalline cellulose with active pharmaceutical ingredients [64]. Furthermore, it is suspected that the Maillard reaction products in MCC can potentially cause a browning effect on the hydrogel film. However, further investigation is required to determine the extent of this effect.

3.8 MCC Application Test as Hydrogel Film Filler

Hydrogel-based polymer is a three-dimensional polymer capable of absorbing water due to its hydrophilic characteristics, resulting in a wide range of applications in food packaging. Hydrogel-based food packaging provides a lot for prospective as green and environmentally friendly packaging [65], as well as the ability to preserve fruits and vegetables fresh. The application of biopolymer-based hydrogel in food packaging is still limited currently, but its beneficial properties, such as biocompatibility, nontoxicity, and biodegradability, make it worthwhile to develop [66]. The hydrogel is typically made as a film and dried to fulfill its features as a water absorber, even though it has good mechanical strength as a fresh food packing film. Research has shown that gelatin-based hydrogels with MCC and NCC can manage moisture and minimize exudates [67]. MCC added to biocomposite film enhances tensile strength, light transmission, and thermal stability while reducing water solubility [40].

The MCC generated under optimal conditions, especially hydrolysis at a concentration of 2.5 N HCl for 45 min, was tested for formulation with carboxymethyl cellulose (CMC) to make a hydrogel. The MCC and CMC composites used in the current research are OPEFB cellulose derivatives. Fig. 10 represents the test at 10% and 20% MCC, which makes the casting process easy and non-torn while remaining elastic and robust. Water absorbs up to 400–600 times its weight.

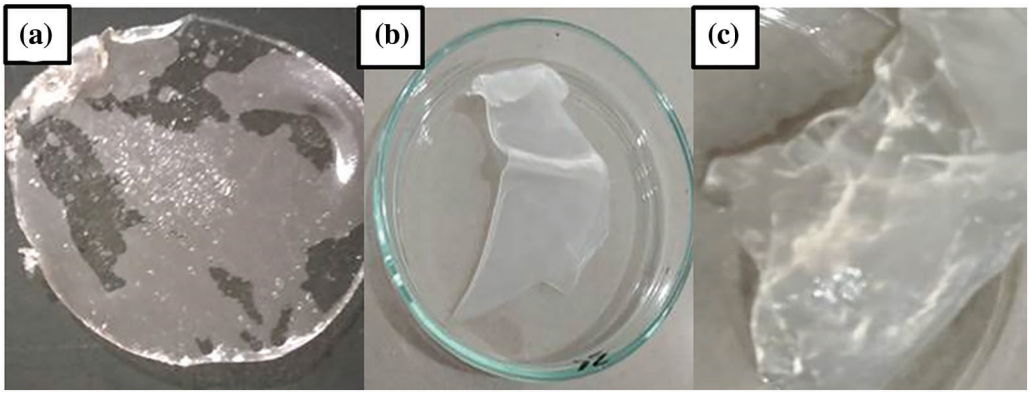

Figure 10: (a) Hydrogel film from MCC and CMC; (b) swelling test of hydrogel film from MCC:CMC 10:90, (c) swelling test of hydrogel film from MCC:CMC 20:80

Hydrogels produced entirely of CMC have low mechanical strength and rupture easily. This indicates that while MCC frequently acts as a filler for tablet reinforcing, it also has the potential to be used as a hydrogel film filler for biowrapping. Previous research has been completed to reinforce the mechanical structure of hydrogel films utilizing CMC composites with synthetic polymers, including CMC with polyvinylpyrrolidone (PVP) [68–70], and CMC with polyethylene oxide [71]. In this research, the evaluation of OPEFB cellulose-based MCC and CMC composites on hydrogel films indicated the MCC's potential for usage as a filler that can boost mechanical strength in certain proportions while maintaining water absorption. More research is required to realize the potential of MCC synthesis from OPEFB.

The mechanical strength of physically connected hydrogels can be improved when the physical interaction between polymer chains is enhanced by increasing the polymer concentration. Alternatively, these hydrogels can be strengthened by forming a liquid crystalline phase in the polymer solution, even at low concentrations, such as through freeze-thaw stages. Forming a liquid crystalline phase increases the mechanical strength of hydrogels through the strong, rigid intermolecular interactions of the liquid-crystalline structure [54]. MCC incorporation in HDPE and cantala fiber composites can significantly increase mechanical strength, including tensile strength, flexural strength, and impact strength [72].

The mechanical strength of the hydrogel film produced can be indicated by the texture during the swelling test or by using the tensile strength test (Table 8). Hydrogel film with CMC/MCC formulation 90:10 has a solid structure after absorbing a certain amount of water and expands the initial 200% and 400% after rehydration of the dry gel. While the hydrogel film with CMC/MCC 80/20 formulation can expand initially up to 600%, and rehydration of the dry gel reaches 1300%. CMC/MCC formula 80: 20 formula is able to absorb water relatively high, expands but decays from its shape, but does not dissolve (Fig. 10).

Table 8: Data of hydrogel characteristics

Formula CMC/ MCC	Swelling (%)	Characteristics	Gel fraction (%)	Gel after rehidration (%)	Tensile strength (Mpa)	Strain at F max (%)
90/10	222.72	gel	10.06	488.46	0.295	48.74
80/20	603.02	soften gel (swinging)	5.87	1314.29	0.237	75.98

In biowrapping, not only are the specifications able to absorb moisture, but also, mechanically, when it comes to water, it is able to maintain its structure. Table 8 shows that the tensile strength of hydrogel film from CMC/MCC formulation 90:10 tends to be higher than CMC/MCC 80:20, but for strain at max force for 80/20 is higher than 90/10. In the future, the suitability of each hydrogel formula, CMC, and MCC will depend on the product application specifications. CMC/MCC formulas 80:20 can be developed at high water absorption levels for the hydrogel, such as absorbent pads in food and non-food products.

4 Conclusions

MCC from OPEFB is one of the potential cellulose derivatives that can be developed. This MCC can be used as a filler in composite products, specifically hydrogels. Hydrogel with specific features has a high water absorption capacity. In using MCC as a hydrogel film filler, MCC should encourage the hydrogen gel so it is not readily dissolved. Therefore, MCC with higher crystallinity and water absorption ability is required to formulate the cellulose-based hydrogel. It was discovered that the higher the concentration of HCl and the longer the hydrolyze performed produced MCC with more excellent crystallinity, while the water absorption capacity was decreased.

Hydrolysis of OPEFB cellulose in 2.5 N HCl for 45 min results in a balanced property with a high degree of crystallinity yet adequate water absorption. The more intense the acid hydrolysis, the larger the crystallites and the greater the loss of the structure. However, the thermal test findings reveal that the MCC of OPEFB in 2.5 N HCl for 45 min still has an amorphous structure, allowing for adequate water absorption. This treatment with CMC resulted in good hydrogel quality in a hydrogel film synthesis test with an MCC composite. Hydrogels may absorb large volumes of water and keep their structure intact without disintegrating.

Acknowledgement: None.

Funding Statement: The authors are grateful for the Universitas Gadjah Mada's financial support for this research. This research was conducted using the Final Project Recognition Grant Universitas Gadjah Mada Indonesia Number of 5075/UN1.P.II/DitLit/PT.01.01/2023.

Author Contributions: SS and MA conceptualized. The methodology was contributed by SS, MA, WW, and MAF. SS and MA managed project administration. Formal analysis was performed by SS, MA, WW, and MAF. SS and MA were responsible for the investigation. SS and MA were engaged in the provision of resources. SS was involved in software development. Validation was provided by SS and MA. SS and MA analyzed the data. SS prepared the initial draft. SS, MA, WW, and MAF reviewed and improved the manuscript. MA designed the graphic design. The study was conducted by MA, WW, and MAF. SS and MA contributed to the acquisition of resources. The manuscript's published version has been read and approved by all authors.

Availability of Data and Materials: This article has no additional data.

Conflicts of Interest: The authors declare that they have no conflicts of interest to report regarding the present study.

References

1. Susi, S., Ainuri, M., Wagiman, W., Fallah, M. A. F. (2023). High-yield alpha-cellulose from oil palm empty fruit bunches by optimizing thermochemical delignification processes for use as microcrystalline cellulose. *International Journal of Biomaterials, 2023(1),* 1–15. https://doi.org/10.1155/2023/9169431
2. Seddiqi, H., Oliaei, E., Honarkar, H., Jin, J., Geonzon, L. C. et al. (2021). Cellulose and its derivatives: Towards biomedical applications. *Cellulose, 28(4),* 1893–1931. https://doi.org/10.1007/s10570-020-03674-w
3. Song, B., Zhao, S., Shen, W., Collings, C., Ding, S. Y. (2020). Direct measurement of plant cellulose microfibril and bundles in native cell walls. *Frontiers in Plant Science, 11(4),* 1–11. https://doi.org/10.3389/fpls.2020.00479
4. Haldar, D., Purkait, M. K. (2020). Micro and nanocrystalline cellulose derivatives of lignocellulosic biomass: A review on synthesis, applications and advancements. *Carbohydrate Polymers, 250(8),* 116937. https://doi.org/10.1016/j.carbpol.2020.116937
5. Morais, J. P. S., Rosa, M. D. F., de Souza Filho, M. D. S. M., Nascimento, L. D., Do Nascimento, D. M. et al. (2013). Extraction and characterization of nanocellulose structures from raw cotton linter. *Carbohydrate Polymers, 91(1),* 229–235. https://doi.org/10.1016/j.carbpol.2012.08.010
6. El-Sakhawy, M., Hassan, M. L. (2007). Physical and mechanical properties of microcrystalline cellulose prepared from agricultural residues. *Carbohydrate Polymers, 67(1),* 1–10. https://doi.org/10.1016/j.carbpol.2006.04.009
7. Tarchoun, A. F., Trache, D., Klapötke, T. M. (2019). Microcrystalline cellulose from Posidonia oceanica brown algae: Extraction and characterization. *International Journal of Biological Macromolecules, 138,* 837–845. https://doi.org/10.1016/j.ijbiomac.2019.07.176
8. Ilindra, A., Dhake, J. D. (2008). Microcrystalline cellulose from bagasse and rice straw. *Indian Journal of Chemical Technology, 15(5),* 497–499.
9. Gusrianto, P., Zulharmita, Z., Rivai, H. (2011). Preparasi dan karakterisasi mikrokristalin selulosa dari limbah serbuk kayu penggergajian. *Jurnal Sains Dan Teknologi Farmasi, 16(2),* 180–188.
10. Setu, M. N. I., Mia, M. Y., Lubna, N. J., Chowdhury, A. A. (2014). Preparation of microcrystalline cellulose from cotton and its evaluation as direct compressible excipient in the formulation of naproxen tablets. *Dhaka University Journal of Pharmaceutical Sciences, 13(2),* 187–192. https://doi.org/10.3329/dujps.v13i2.21899
11. Merci, A., Urbano, A., Grossmann, M. V. E., Tischer, C. A., Mali, S. (2015). Properties of microcrystalline cellulose extracted from soybean hulls by reactive extrusion. *Food Research International, 73,* 38–43. https://doi.org/10.1016/j.foodres.2015.03.020
12. Rizkiansyah, R. R., Mardiyati, S., Suratman, R. (2016). Crystallinity and thermal resistance of microcrystalline cellulose prepared from manau rattan (Calamusmanan). *AIP Conference Proceedings, 1725(4),* 1–6. https://doi.org/10.1063/1.4945525
13. Owolabi, A. F., Haafiz, M. K. M., Hossain, M. S., Hussin, M. H., Fazita, M. R. N. (2017). Influence of alkaline hydrogen peroxide pre-hydrolysis on the isolation of microcrystalline cellulose from oil palm fronds. *International Journal of Biological Macromolecules, 95,* 1228–1234. https://doi.org/10.1016/j.ijbiomac.2016.11.016

14. Ahmad, Z., Roziaizan, N. N., Rahman, R., Mohamad, A. F., Wan Ismail, W. I. N. (2016). Isolation and characterization of microcrystalline cellulose (MCC) from rice husk (RH). *MATEC Web of Conferences, 47,* 1–6. https://doi.org/10.1051/matecconf/20164705013
15. Shao, X., Wang, J., Liu, Z., Hu, N., Liu, M. et al. (2020). Preparation and characterization of porous microcrystalline cellulose from corncob. *Industrial Crops and Products, 151,* 112457 1–6. https://doi.org/10.1016/j.indcrop.2020.112457
16. Kunusa, W. R., Iyabu, H., Taufik, M., Botutihe, D. N. (2018). Characterization and analysis of the molecular weight of corn corbs microcrystalline cellulose (MCC) fiber using mass-spectrometry methods. *IOP Conference Series: Journal of Physics, 1040,* 012015. https://doi.org/10.1088/1742-6596/1040/1/012015
17. Roro, R., Yusrina, A., Suryadi, H. (2018). Preparation and characterization of microcrystalline cellulose produced from betung bamboo (*Dendrocalamus asper*) through acid hydrolysis. *Journal of Young Pharmacists, 10(2),* 79–83. https://doi.org/10.5530/jyp.2018.2s.15
18. Emeje, M., Ekpo, M., Olayemi, O., Isimi, C., Buraghoin, A. (2020). Physicochemical and drug release properties of microcrystalline cellulose derived from *Musa balbisiana*. *Polimeros-Ciencia E Tecnologia, 30(1),* 1–6. https://doi.org/10.1590/0104-1428.07418
19. Edison, D. A., Sari, E. D. (2019). Karakteristik selulosa mikrokristalin dari rumput laut merah Eucheuma cottonii. *Indonesian Fisheries Processing Journal, 22(3),* 483–489. https://doi.org/10.17844/jphpi.v22i3.28946
20. Nasution, H., Harahap, H., Suherman, P., Kelvin, K. (2020). Isolation and characterization of microcrystalline cellulose from coconut fiber using acid hydrolysis process. *Proceedings of ICOSTEERR, International Conference of Science, Technology, Engineering, Environmental and Ramification Researches*, vol. 1, pp. 222–226. Universitas Sumatera Utara, Medan, Indonesia. https://doi.org/10.5220/0010077802220226
21. Fouad, H., Kian, L. K., Jawaid, M., Alotaibi, M. D., Alothman, O. Y. et al. (2020). Characterization of microcrystalline cellulose isolated from conocarpus fiber. *Polymers, 12(12),* 1–11. https://doi.org/10.3390/polym12122926
22. Haafiz, M. K. M., Eichhorn, S. J., Hassan, A., Jawaid, M. (2013). Isolation and characterization of microcrystalline cellulose from oil palm biomass residue. *Carbohydrate Polymers, 93(2),* 628–634. https://doi.org/10.1016/j.carbpol.2013.01.035
23. Ramli, R., Junadi, N., Beg, M. D. H., Yunus, R. M. (2015). Microcrystalline cellulose (MCC) from oil palm empty fruit bunch (EFB) fiber via simultaneous ultrasonic and alkali treatment. *International Journal of Materials and Metallurgical Engineering, 9(1),* 8–11. https://doi.org/10.5281/zenodo.1337783
24. Ismail, F., Othman, N. E. A., Wahab, N. A., Hamid, F. A., Aziz, A. A. (2021). Preparation of microcrystalline cellulose from oil palm empty fruit bunch fibre using steam-assisted acid hydrolysis. *Journal of Advanced Research in Fluid Mechanics and Thermal Sciences, 81(1),* 88–98. https://doi.org/10.37934/arfmts.81.1.8898
25. Lai, D. S., Osman, A. F., Adnan, S. A., Ibrahim, I., Alrashdi, A. A. et al. (2021). On the use of OPEFB-derived microcrystalline cellulose and nano-bentonite for development of thermoplastic starch hybrid bio-composites with improved performance. *Polimers, 13(897),* 1–22. https://doi.org/10.3390/polym13060897
26. Owolabi, A. F., Ghazali, A., Khalil, H. P. S. A., Hassan, A., Arjmandi, R. et al. (2016). Isolation and characterization of microcrystalline cellulose from oil palm fronds using chemomechanical process. *Wood and Fiber Science, 48(4),* 260–270.
27. Biby, G., Hanna, M., Miladinov, V. (2001). Production of microcrystalline cellulose by reactive extrusion (US 6228213B1). https://patents.google.com/patent/US6228213/ar
28. Holilah, H., Prasetyoko, D., Ediati, R., Bahruji, H., Jalil, A. A. et al. (2021). Hydrothermal assisted isolation of microcrystalline cellulose from pepper (*Piper nigrum L.*) processing waste for making sustainable bio-composite. *Journal of Cleaner Production, 305,* 127229. https://doi.org/10.1016/j.jclepro.2021.127229
29. Ventura-Cruz, S., Tecante, A. (2019). Extraction and characterization of cellulose nanofibers from Rose stems (*Rosa* spp.). *Carbohydrate Polymers, 220,* 53–59. https://doi.org/10.1016/j.carbpol.2019.05.053
30. Sharma, A., Thakur, M., Bhattacharya, M., Mandal, T., Goswami, S. (2019). Commercial application of cellulose nano-composites–A review. *Biotechnology Reports, 21,* e00316. https://doi.org/10.1016/j.btre.2019.e00316

31. Ching, Y. C., Ng, T. S. (2014). Effect of preparation conditions on cellulose from oil palm empty fruit bunch fiber. *BioResources, 9(4),* 6373–6385. https://doi.org/10.15376/biores.9.4.6373-6385
32. Trache, D., Hussin, M. H., Hui Chuin, C. T., Sabar, S., Fazita, M. R. N. et al. (2016). Microcrystalline cellulose: Isolation, characterization and bio-composites application—A review. *International Journal of Biological Macromolecules, 93,* 789–804. https://doi.org/10.1016/j.ijbiomac.2016.09.056
33. Kundu, D., Banerjee, T. (2020). Development of microcrystalline cellulose based hydrogels for the *in vitro* delivery of Cephalexin. *Heliyon, 6(1),* e03027. https://doi.org/10.1016/j.heliyon.2019.e03027
34. Dai, H., Chen, Y., Ma, L., Zhang, Y., Cui, B. (2021). Direct regeneration of hydrogels based on lemon peel and its isolated microcrystalline cellulose: Characterization and application for methylene blue adsorption. *International Journal of Biological Macromolecules, 191(2),* 129–138. https://doi.org/10.1016/j.ijbiomac.2021.09.063
35. Nie, G., Zang, Y., Yue, W., Wang, M., Baride, A. et al. (2021). Cellulose-based hydrogel beads: Preparation and characterization. *Carbohydrate Polymer Technologies and Applications, 2(4),* 1–11. https://doi.org/10.1016/j.carpta.2021.100074
36. Maturi, M., Spanu, C., Baschieri, A., Comes Franchini, M., Locatelli, E. et al. (2022). Iridium-functionalized cellulose microcrystals as a novel luminescent biomaterial for biocomposites. *Biomolecules, 12(9),* 1–14. https://doi.org/10.3390/biom12091165
37. Zhao, H., Zhang, K., Rui, S., Zhao, P. (2020). Study on microcrystalline cellulose/chitosan blend foam gel material. *Science and Engineering of Composite Materials, 27(1),* 424–432.
38. Ventura-Cruz, S., Tecante, A. (2021). Nanocellulose and microcrystalline cellulose from agricultural waste: Review on isolation and application as reinforcement in polymeric matrices. *Food Hydrocolloids, 118,* 106771. https://doi.org/10.1016/j.foodhyd.2021.106771
39. Costa, L. V., Iulianelli, G. C. V., da Silva, P. S. R. C., dos Santos, F. A. (2021). Obtaining and characterization of biodegradable composites reinforced with microcrystalline cellulose fillers. *Materials Sciences and Applications, 12(12),* 561–577. https://doi.org/10.4236/msa.2021.1212037
40. Ren, H., Li, S., Gao, M., Xing, X., Tian, Y. et al. (2023). Preparation and characterization of microcrystalline cellulose/polylactic acid biocomposite films and its application in Lanzhou lily (*Lilium davidii var. unicolor*) bulbs preservation. *Sustainability, 15(18),* 1–18. https://doi.org/10.3390/su151813770
41. Aiman, M., Amalina, N., Amira, N., Najwa, K., Amin, M. et al. (2020). Materials Today : Proceedings Characterization and property investigation of microcrystalline cellulose (MCC) and carboxymethyl cellulose (CMC) filler on the carrageenan-based biocomposite film. *Materials Today: Proceedings, 42(2),* 1–7. https://doi.org/10.1016/j.matpr.2020.09.304
42. Li, M., Wei, T., Qian, C., Liang, Z. (2021). Preparation of microcrystalline cellulose from *Rabdosia rubescens* residue and study on its membrane properties. *Scientific Reports, 11(1),* 1–9. https://doi.org/10.1038/s41598-021-98645-x
43. Tasnim, S., Tipu, M. F. K., Rana, M. S., Rahim, M. A., Haque, M. et al. (2023). Modification of bulk density, flow property and crystallinity of microcrystalline cellulose prepared from waste cotton. *Materials, 16(16),* 1–12. https://doi.org/10.3390/ma16165664
44. Ohwoavworhua, F., Adelakun, T., Okhamafe, A. (2009). Processing pharmaceutical grade microcrystalline cellulose from groundnut husk: Extraction methods and characterization. *International Journal of Green Pharmacy, 3(2),* 97–104. https://doi.org/10.4103/0973-8258.54895
45. Segal, L., Creely, J. J., Martin, A. E., Conrad, C. M. (1959). An empirical method for estimating the degree of crystallinity of native cellulose using the X-ray diffractometer. *Textile Research Journal, 29(10),* 786–794. https://doi.org/10.1177/004051755902901003
46. Huang, X., Xie, F., Xiong, X. (2018). Surface-modified microcrystalline cellulose for reinforcement of chitosan film. *Carbohydrate Polymers, 201(8),* 367–373. https://doi.org/10.1016/j.carbpol.2018.08.085
47. De Souza Lima, M. M., Borsali, R. (2004). Rodlike cellulose microcrystals: Structure, properties, and applications. *Macromolecular Rapid Communications, 25(7),* 771–787. https://doi.org/10.1002/marc.200300268

48. Sun, C. C. (2008). Mechanism of moisture induced variations in true density and compaction properties of microcrystalline cellulose. *International Journal of Pharmaceutics, 346(1–2),* 93–101. https://doi.org/10.1016/j.ijpharm.2007.06.017
49. Nwachukwu, N., Ofoefule, S. I. (2020). Effect of drying methods on the powder and compaction properties of microcrystalline cellulose derived from gossypium herbaceum. *Brazilian Journal of Pharmaceutical Sciences, 56,* 1–17. https://doi.org/10.1590/s2175-97902020000118060
50. Prusov, A. N., Prusova, S. M., Radugin, M. V., Zakharov, A. G. (2014). Interrelation between the crystallinity of polysaccharides and water absorption. *Russian Journal of Physical Chemistry A, 88(5),* 813–818. https://doi.org/10.1134/S0036024414050239
51. Sun, Y., Lin, L., Deng, H., Li, J., He, B. et al. (2008). Structural changes of bamboo cellulose in formic acid. *BioResources, 3(2),* 297–315. https://doi.org/10.15376/biores.3.2.297-315
52. Yohana Chaerunisaa, A., Sriwidodo, S., Abdassah, M. (2020). Microcrystalline cellulose as pharmaceutical excipient. In: *Pharmaceutical formulation design-recent practices*, pp. 1–21. London, UK: IntechOpen. https://doi.org/10.5772/intechopen.88092
53. Zeng, P., Chen, X., Qin, Y. R., Zhang, Y. H., Wang, X. P. et al. (2019). Preparation and characterization of a novel colorimetric indicator film based on gelatin/polyvinyl alcohol incorporating mulberry anthocyanin extracts for monitoring fish freshness. *Food Research International, 126(8),* 108604 1–8. https://doi.org/10.1016/j.foodres.2019.108604
54. Kang, H., Song, X., Wang, Z., Zhang, W., Zhang, S. et al. (2016). High-performance and fully renewable soy protein isolate-based film from microcrystalline cellulose via bio-inspired poly(dopamine) surface modification. *ACS Sustainable Chemistry and Engineering, 4(8),* 4354–4360. https://doi.org/10.1021/acssuschemeng.6b00917
55. Beroual, M., Boumaza, L., Mehelli, O., Trache, D., Tarchoun, A. F. et al. (2021). Physicochemical properties and thermal stability of microcrystalline cellulose isolated from Esparto grass using different delignification approaches. *Journal of Polymers and the Environment, 29(1),* 130–142. https://doi.org/10.1007/s10924-020-01858-w
56. Baruah, J., Deka, R. C., Kalita, E. (2020). Greener production of microcrystalline cellulose (MCC) from Saccharum spontaneum (Kans grass): Statistical optimization. *International Journal of Biological Macromolecules, 154,* 672–682. https://doi.org/10.1016/j.ijbiomac.2020.03.158
57. Jahan, M. S., Saeed, A., He, Z., Ni, Y. (2011). Jute as raw material for the preparation of microcrystalline cellulose. *Cellulose, 18(2),* 451–459. https://doi.org/10.1007/s10570-010-9481-z
58. Li, R., Fei, J., Cai, Y., Li, Y., Feng, J. et al. (2009). Cellulose whiskers extracted from mulberry: A novel biomass production. *Carbohydrate Polymers, 76(1),* 94–99. https://doi.org/10.1016/j.carbpol.2008.09.034
59. Ng, H. M., Sin, L. T., Tee, T. T., Bee, S. T., Hui, D. et al. (2015). Extraction of cellulose nanocrystals from plant sources for application as reinforcing agent in polymers. *Composites Part B: Engineering, 75,* 176–200. https://doi.org/10.1016/j.compositesb.2015.01.008
60. Ciolacu, D., Ciolacu, F., Popa, V. I. (2011). Amorphous cellulose-structure and characterization. *Cellulose Chemistry and Technology, 45(1–2),* 13–21.
61. Kassem, I., Kassab, Z., Khouloud, M., Sehaqui, H., Bouhfid, R. et al. (2020). Phosphoric acid-mediated green preparation of regenerated cellulose spheres and their use for all-cellulose cross-linked superabsorbent hydrogels. *International Journal of Biological Macromolecules, 162,* 136–149. https://doi.org/10.1016/j.ijbiomac.2020.06.136
62. Azubuike, C. P., Okhamafe, A. O. (2012). Physicochemical, spectroscopic and thermal properties of microcrystalline cellulose derived from corn cobs. *International Journal of Recycling of Organic Waste in Agriculture, 1(1),* 106–115. https://doi.org/10.1186/2251-7715-1-9
63. Gichuki, J., Kareru, P. G., Gachanja, A. N., Ngamau, C. (2022). Characteristics of microcrystalline cellulose from coir fibers. *Journal of Natural Fibers, 19(3),* 915–930. https://doi.org/10.1080/15440478.2020.1764441
64. Wu, Y., Levons, J., Narang, A. S., Raghavan, K., Rao, V. M. (2011). Reactive impurities in excipients: Profiling, identification and mitigation of drug-excipient incompatibility. *AAPS PharmSciTech, 12(4),* 1248–1263. https://doi.org/10.1208/s12249-011-9677-z

65. Huang, K., Wang, Y. (2022). Recent applications of regenerated cellulose films and hydrogels in food packaging. *Current Opinion in Food Science, 43,* 7–17. https://doi.org/10.1016/j.cofs.2021.09.003
66. Nguyen, M. K., Lee, D. S. (2010). Injectable biodegradable hydrogels. *Macromolecular Bioscience, 10(6),* 563–579. https://doi.org/10.1002/mabi.200900402
67. Acevedo-Puello, V., Figueroa-López, K. J., Ortega-Toro, R. (2023). Gelatin-based hydrogels containing microcrystalline and nanocrystalline cellulose as moisture absorbers for food packaging applications. *Journal of Composites Science, 7(8),* 1–14. https://doi.org/10.3390/jcs7080337
68. Roy, N., Saha, N., Kitano, T., Saha, P. (2012). Biodegradation of PVP-CMC hydrogel film: A useful food packaging material. *Carbohydrate Polymers, 89(2),* 346–353. https://doi.org/10.1016/j.carbpol.2012.03.008
69. Gregorova, A., Saha, N., Kitano, T., Saha, P. (2015). Hydrothermal effect and mechanical stress properties of carboxymethylcellulose based hydrogel food packaging. *Carbohydrate Polymers, 117,* 559–568. https://doi.org/10.1016/j.carbpol.2014.10.009
70. Bandyopadhyay, S., Saha, N., Zandraa, O., Pummerova, M., Saha, P. (2020). Essential oil based PVP-CMC-BC-GG functional hydrogel sachet for ' Cheese ': Its shelf life confirmed with anthocyanin (isolated from red cabbage) bio stickers. *Foods, 9(3),* 1–20. https://doi.org/10.3390/foods9030307
71. Kanafi, N. M., Rahman, N. A., Rosdi, N. H. (2019). Citric acid cross-linking of highly porous carboxymethyl cellulose/poly (ethylene oxide) composite hydrogel films for controlled release applications. *Materials Today: Proceedings, 7,* 721–731. https://doi.org/10.1016/j.matpr.2018.12.067
72. Raharjo, W. W., Salam, R., Ariawan, D. (2023). The Effect of microcrystalline cellulose on the physical, thermal, and mechanical properties of composites based on Cantala fiber and recycled high-density polyethylene. *Journal of Natural Fibers, 20(2),* 1–16. https://doi.org/10.1080/15440478.2023.2204454